Effect of Copper−Ceria Interactions on Copper Reduction in a $Cu/CeO_2/Al_2O_3$ Catalyst Subjected to Thermal Treatments in CO

Arturo Martínez-Arias, Renato Cataluña,† José C. Conesa, and Javier Soria*

Instituto de Catálisis y Petroleoquímica, CSIC, Campus Universitario de Cantoblanco, Camino de Valdelatas s/n, 28049 Madrid, Spain

Received: June 30, 1997; In Final Form: November 1, 1997

A comparative study of Cu/Al_2O_3 (CuA) and $Cu/CeO_2/Al_2O_3$ (CuCA) catalysts, examining the redox processes induced by thermal treatments in CO on preoxidized samples, has been performed by means of temperature-programmed techniques (TPR, TPO, and TPD) and FTIR and EPR spectroscopies. The results evidence different chemical behaviors of the copper entities as a function of their dispersion degree and interactions with the different components of the support. For CuA, three types of Cu^{2+} entities are evidenced, showing different dispersion degree and different reducibilities in CO. Clustered Cu^{2+} species are shown to be more easily reduced than isolated Cu^{2+} ions. For CuCA, part of the copper ions interact with the ceria component, as revealed in the initial calcined samples by the lower overall intensity of Cu^{2+} observed by EPR and by the formation of specific surface carbonyl complexes, upon CO adsorption, giving an FTIR band at 2105 cm^{-1}. These results are attributed to the presence of copper ions, interacting with large three-dimensional-like ceria particles (3D-Ce), which are reduced by CO at $T_r \leq 473$ K, yielding metallic copper particles evidenced by specific carbonyl bands in the FTIR spectra. The results also indicate that the reduction of the copper species located in contact with more dispersed two-dimensional-like ceria entities (2D-Ce) can be favored by the effect of this contact. This easier reduction of copper interacting with ceria is presumed to favor the catalytic activity of CuCA for CO oxidation.

Introduction

Cerium oxide is widely used as a promoter in the so-called "three-way catalysts" (TWC) for the elimination of toxic exhaust gases in automobiles, in which the active component is mainly formed by platinum group metals dispersed on CeO_2/Al_2O_3 supports.[1] The promoting effect of cerium oxide is believed to include both structural aspects, like the enhancement of the metal dispersion and the stabilization of the γ-Al_2O_3 support toward thermal sintering,[2] and chemical ones, like the enhancement of the oxygen storage capacity of the systems[3] or its participation in the water-gas shift reaction[4] or in the decomposition of nitrogen oxides.[5] More recent efforts are devoted to elucidate the participation of ceria in important metal/support interactions that can substantially affect catalyst properties.[6] It is generally recognized that these interactions are mainly responsible for the important promoting effect of ceria on these systems, these effects being connected to the particular redox properties acquired by the systems upon establishment of metal−ceria contacts.[7]

In this sense, considering systems containing both copper and ceria, formation of intimate copper−ceria contacts is thought to be of crucial importance to explain the remarkably high activities exhibited for methanol synthesis[8] or for carbon monoxide oxidation.[9,10] In the case of using alumina-supported ceria systems as supports for copper, several questions arise in principle from the fact that the structure of ceria can change as a function of its dispersion and/or of its interactions with the alumina support,[11,12] and in addition, copper can also appear forming clusters or as isolated cations in the calcined samples;[10] as a consequence, different metal−support interactions would presumably be present upon incorporation of copper on these supports depending on the characteristics of the copper or ceria entities. Previous works have shown that at least two different types of ceria entities can be discerned in alumina-supported ceria systems.[11,12] One would consist in highly dispersed ceria entities (called 2D-Ce), which would experience important interactions with the alumina support and would consequently show significant differences in chemical behavior, with respect to pure ceria.[11−13] The other entities are relatively large three-dimensional ceria particles (called 3D-Ce); these would present properties closer to those of pure ceria, although one could still expect some differences between different ceria particles as a function of their size.[14]

A recent report[10] has shown that the catalytic activity of $Cu/CeO_2/Al_2O_3$ systems for CO oxidation is improved by increasing the ceria content of the catalysts, thus suggesting that the promoting effect observed depends mainly on copper interactions with relatively large three-dimensional ceria particles, although certain influence of copper interacting with dispersed ceria entities was inferred as well from the analyses of the reactivity profiles obtained. In this contribution, two of the catalysts used in that previous study of catalytic activity for CO oxidation[10] are examined; it was observed there that the incorporation of ceria to the catalyst produced an important promotion of the catalytic activity, the $Cu/CeO_2/Al_2O_3$ catalyst showing isoconversion temperatures ca. 200 K lower than the Cu/Al_2O_3 catalyst.[10] Among the aspects that might affect the reactivity of these systems, it is worth considering the influence of copper−support interactions on the redox behavior of copper, particularly taking into account that the activity of this base

† Present address: Escola de Engenharia, Departamento de Engenharia Química, UFRGS, Brazil.

* Corresponding author. E-mail jsoria@icp.csic.es; Fax 34 1 5854760.

S1089-5647(97)02097-X CCC: $15.00
Published on Web 01/29/1998

metal for reactions of interest in the TWC field, like CO oxidation, increases with its reduction degree.[15]

Experimental Section

Materials. A CeO_2/Al_2O_3 support (with a final load in CeO_2 = 10 wt %) was prepared by incipient wetness impregnation of γ-Al_2O_3 (as 1.8 mm diameter spheres, supplied by Condea, S_{BET} = 200 m^2 g^{-1}) with an aqueous solution of $Ce(NO_3)_3 \cdot 6H_2O$. The resulting material was dried overnight at 353 K and subsequently calcined at 773 K under a dry air flow for 6 h. Copper (to a final load of 1 wt %) was incorporated by impregnation of the supports (Al_2O_3 or CeO_2/Al_2O_3) with aqueous solutions of $Cu(NO_3)_2 \cdot 3H_2O$ (Merck, 99.5% purity). To decompose the deposited complex, the samples were dried and calcined in the same conditions described above for the CeO_2/Al_2O_3 support. Except for the CO-TPR experiments where 0.4−0.5 mm particles were selected after crushing and sieving (previous results showed the absence of internal diffusion effects in this case[16]), the samples were ground into powder with an agate mortar. Samples CeO_2/Al_2O_3, Cu/Al_2O_3, and $Cu/CeO_2/Al_2O_3$ will be hereafter referred to as CA, CuA, and CuCA, respectively. All the gases employed were of commercial purity and, for adsorption experiments, were further purified, before storage, by vacuum distillation methods.

Techniques. EPR spectra were recorded at 77 K with a Bruker ER 200 D spectrometer operating in the X-band and calibrated with a DPPH standard (g = 2.0036). Computer simulations were used in some cases to check spectral parameters or determine the relative magnitude of overlapping signals. Portions of about 40 mg of sample were placed inside a special quartz probe cell with greaseless stopcocks, using a conventional high-vacuum line (capable of maintaining a dynamic vacuum of ca. 6×10^{-3} N m^{-2}) for the different treatments. For the oxygen adsorption experiments at T_a = 77 K, doses of about 70 μmol/g were used. CO reduction treatments were made in static conditions using 100 Torr of CO, heating during 1 h at the corresponding reduction temperature (T_r), and subsequently outgassing at the same temperature for 0.5 h.

FTIR spectra were recorded at room temperature with a Nicolet 5ZDX Fourier transform spectrometer, with a resolution of 4 cm^{-1} and taking 128 scans for every spectrum. Thin self-supporting disks (ca. 10 mg cm^{-2}) were prepared and handled in standard greaseless cells provided with NaCl windows, where they could be subjected to thermal or adsorption treatments. Reduction treatments in CO were performed in the same conditions described above for the EPR experiments.

For the temperature-programmed reduction under CO experiments (CO-TPR), ca. 5 g of sample was placed in a quartz flow reactor. After a standard precalcination treatment consisting of heating under a 3% O_2:N_2 flow at 673 K during 1 h, cooling in the same gas flow to room temperature, and then purging briefly (5 min) with N_2, the mixture is switched to a 1% CO/N_2 mixture at a gas flow rate of 200 cm^3 min^{-1}, and after a short equilibration time, a programmed temperature ramp is initiated at a rate of 5 K min^{-1} up to 973 K, monitoring the evolved gases every 5 K. The analysis of the feed and outlet gas streams was performed using a Perkin-Elmer FT-IR spectrometer model 1725X, coupled to a multiple reflection transmission cell (Infrared Analysis Inc. "long path gas minicell", 2.4 m path length, ca. 130 cm^3 internal volume); O_2 concentration was determined with a paramagnetic analyzer (Servomex 540 A). Temperature-programmed oxidation (TPO) or temperature-programmed desorption (TPD) experiments were performed using 1% O_2/N_2 or pure N_2, respectively, at a rate of 200 cm^3 min^{-1}.

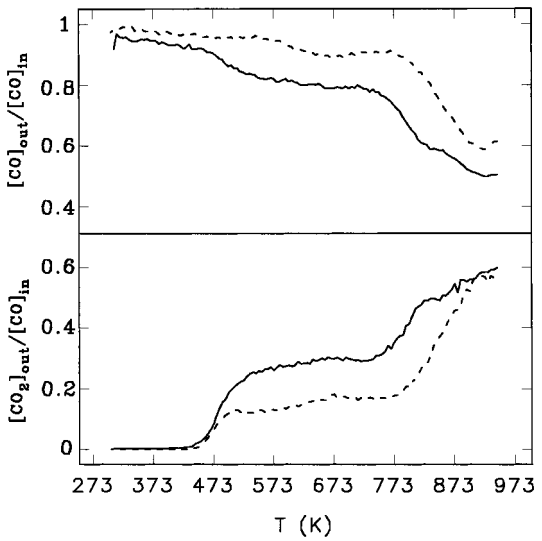

Figure 1. CO-TPR profiles for the CuCA (solid lines) and CuA (dashed lines) catalysts.

TABLE 1: Preliminary Characterization Results Obtained on the Samples Used in This Study

sample	S_{BET} (m^2 g^{-1})	XRD
CA	197	γ-Al_2O_3, CeO_2
CuA	190	γ-Al_2O_3
CuCA	178	γ-Al_2O_3, CeO_2

SEM-EDAX data were taken with a ISI DS-130 system, with an electron acceleration voltage of 20 keV, detection of secondary electrons, and a Si(Li) detector-based Kevex analyzer. The theoretical resolution of the system is calculated to be around 10 nm.

Powder X-ray diffraction patterns were recorded on a Seifert diffractometer using nickel-filtered Cu Kα radiation.

Results

Overall Structural Data. Some preliminary characterization data are summarized in Table 1. It is worth noting that no features that could be related to Cu-containing phases were revealed by XRD. Diffraction peaks corresponding to the CeO_2 fluorite structure were present in the ceria-containing samples; their line widths indicate average crystallite sizes (deduced through application of Scherrer's formula) in the 8−10 nm range, similar in both CA and CuCA samples.

Examination with SEM and EDAX showed that part of the ceria component is homogeneously distributed on the alumina surface and part forms agglomerates with sizes in the 100−200 nm range. Cu appears as rather homogeneously distributed in the CuA sample; in the CuCA sample, it presents variations in concentration, which seems to be higher in the regions richer in Ce.

Temperature-Programmed Experiments. Figure 1 shows the CO-TPR curves obtained on CuA and CuCA samples. A small degree of CO consumption, without CO_2 release, is observed immediately after beginning the TPR runs on both samples, suggesting that some CO is forming adsorbed species. A more important CO consumption is produced at temperatures higher than ca. 423 or 573 K for CuCA or CuA, respectively, being larger for CuCA. A first step of CO_2 production starts at ca. 423 and 453 K for CuCA and CuA, respectively, being comparatively stronger for CuCA. Larger CO consumption−CO_2 production steps are detected at 723 and 773 K for CuCA

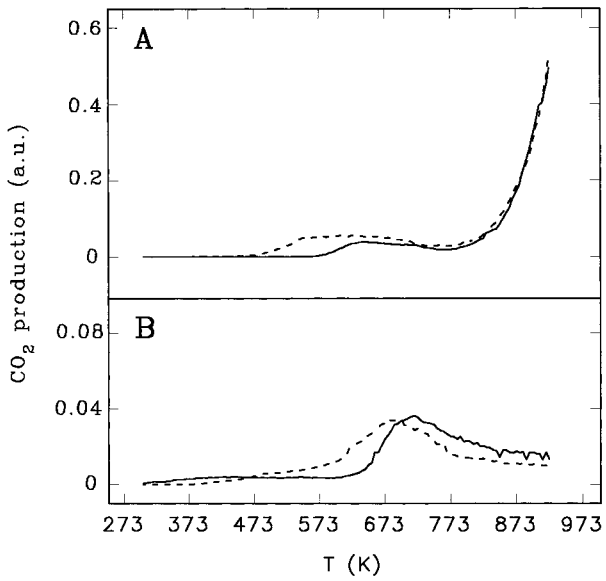

Figure 2. TPO (A) and TPD (B) experiments performed subsequent to CO-TPR experiments on the CuCA (solid lines) and CuA (dashed lines) catalysts.

and CuA, respectively. At the end of the runs, a significant blackening of both samples was observed.

To perform a thorough analysis of these profiles, several processes leading to CO consumption/CO_2 production phenomena should be considered. Thus, in addition to the simple CO + $O_s \rightarrow CO_2$ reduction process (where O_s denotes a surface oxygen atom), the water-gas shift reaction, involving CO and surface hydroxyl groups, or CO disproportionation (Boudouard reaction: $2CO \rightarrow CO_2 + C$) should also be taken into consideration. To study whether the color change might be produced by carbon deposition following the Boudouard reaction or by changes in the oxidation state of copper, the catalysts were studied, directly after completing these CO-TPR runs, by means of TPO experiments. Figure 2A presents CO_2 production curves obtained in these TPO runs, both samples showing a small release in the 473−773 K range and a far more important CO_2 release at $T > 773$ K. At the end of these TPO experiments the samples had recovered their initial colors, pale blue and pale green for CuA and CuCA, respectively. To complete the analysis, CO-TPR runs in conditions similar to the first ones were done, after which TPD experiments (Figure 2B) were performed for both samples to determine whether some of the peaks observed during the TPO runs might be attributed just to decomposition of adsorbed species. No color change is detected at the end of these TPD experiments, the samples remaining black. A small amount of CO (not shown) is as well detected during these TPD runs showing a peak at around 423 K for both samples and at around 700 K for CuCA; it might be attributed to desorption of CO chemisorbed during cooling of the sample in the preceding TPR experiment.[17] These TPD results suggest that the peaks appearing below 773 K in the TPO runs can be partly due to decomposition of adsorbed species, like carbonate or formate species,[18] the formation of which is verified by FTIR as shown below.

FTIR Spectra. In the FTIR spectral regions corresponding to hydroxyls (4000−3000 cm^{-1}) or carbonates (below 1800 cm^{-1}, although the analysis is restricted to wavenumbers higher than 1200 cm^{-1} due to the alumina cutoff), no marked differences are observed between CuA or CuCA samples in the initial calcined state or after being subjected to reductions treatments in CO up to $T_r = 573$ K. Figure 3 shows some typical spectra in these zones. Bands in the 4000−3000 cm^{-1} regions of the spectra can be ascribed in all cases to hydroxyl groups associated to the γ-Al_2O_3 part of the samples; no band unambiguously ascribable to hydroxyls associated to ceria or to oxidized copper entities could be discerned. According to previous studies,[13,19−21] the wide bands detected in the 3600−3500 cm^{-1} zone can be attributed to H-bonded (associated) hydroxyl groups, bands at 3690−3675 cm^{-1} are ascribed to tribridged isolated hydroxyls, those at 3737−3728 cm^{-1} are assigned to bibridged OH^- groups, and shoulders at ca. 3760 cm^{-1} are due to terminal OH^- groups. A certain decrease in the overall intensity of the hydroxyl bands is produced with the increase of T_r, which affected particularly to associated hydroxyl groups while the shoulder at ca. 3760 cm^{-1} due to terminal OH^- groups appeared.

Several intense bands are observed as well at wavenumbers lower than 1800 cm^{-1}. The analysis of the spectra in this zone is complicated by the alumina cutoff, which hinders observation of bands at wavenumbers lower than about 1200 cm^{-1}, and by the possibility that different species of the carbonate type might be present. The spectra of the initial calcined samples show broad bands centered in the 1700−1500 cm^{-1} range and at ca. 1470 cm^{-1}, while weaker peaks are detected at lower wavenumbers. In view of their broadness, these bands can be only tentatively assigned to different carbonate (or bicarbonate) species formed on alumina[18] or oxidized copper entities[22] and produced probably by interaction with atmospheric CO_2 during preparation or storage of the samples. Sharp bands at 1596 and 1388 cm^{-1} (with a shoulder at 1376 cm^{-1}) and a weaker one at 2911 cm^{-1} (not shown), due to formate species on alumina,[23] are produced upon reduction in CO, their intensity increasing with T_r.

Adsorption of a small amount of CO at room temperature on the samples either in their initial calcined state or after being subjected to reduction treatments in CO (following by outgassing at the same temperature) produces only changes in the carbonyl stretching region of the spectra, where new bands are formed as shown in Figure 4. Adsorption of CO on the initial calcined samples show differences between both Cu-containing samples. Thus, while CuA shows two weak bands at 2116 and 2097 cm^{-1}, for CuCA a broad, comparatively more intense band centered at 2105 cm^{-1} is detected. No important differences between both samples are observed in respect to positions of the main FTIR bands detected after CO reduction treatments up to $T_r = 573$ K. These can be classified into three groups appearing at 2097−2105, 2116−2126, and 2135−2143 cm^{-1}. It should be noted however that, as T_r is increased, new small shoulders at 2086 and 2063 cm^{-1} can be detected for CuCA (Figure 4b). These are more clearly revealed by performing spectra subtraction, as shown in the inset of Figure 4, which reveals also the formation of a relatively higher amount of carbonyl bands with wavenumbers above 2100 cm^{-1} on CuCA after treatment in CO at $T_r = 473$ K. An overall intensity decrease of carbonyl bands is observed in both samples for the reduction treatment at $T_r = 573$ K.

It is generally acknowledged that carbonyl bands at wavenumbers lower than about 2110 cm^{-1} are due to carbonyl species adsorbed on metallic copper particles,[24] the variations in their wavenumbers being related to changes in the nature of the exposed metallic copper faces[24] or, in the case of supported catalysts, to differences in the interactions of the metallic copper particles with the underlying support.[25,26] On this basis, bands appearing at 2105−2095 cm^{-1} can be ascribed to carbonyl species adsorbed on metallic copper, while the low wavenumber

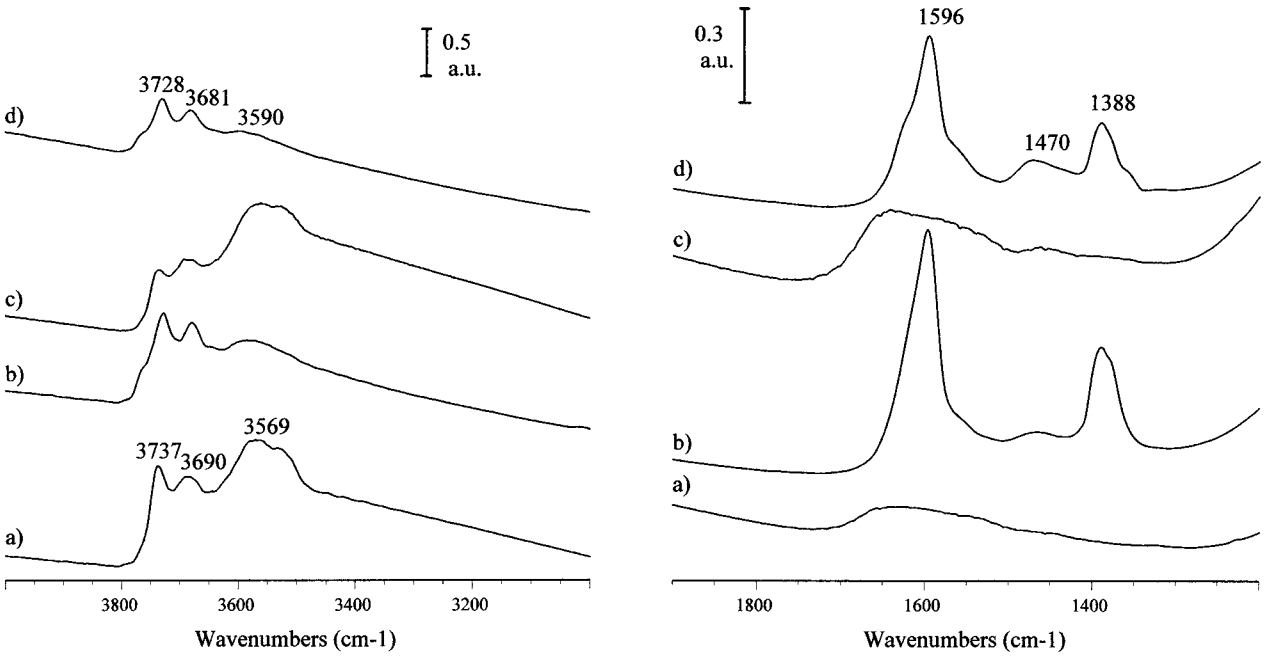

Figure 3. FTIR spectra, separated in different spectral regions, of CuCA and CuA after the following treatments; (a) initial calcined CuCA, (b) CuCA reduced in CO at $T_r = 573$ K, (c) initial calcined CuA, (d) CuA reduced in CO at $T_r = 573$ K.

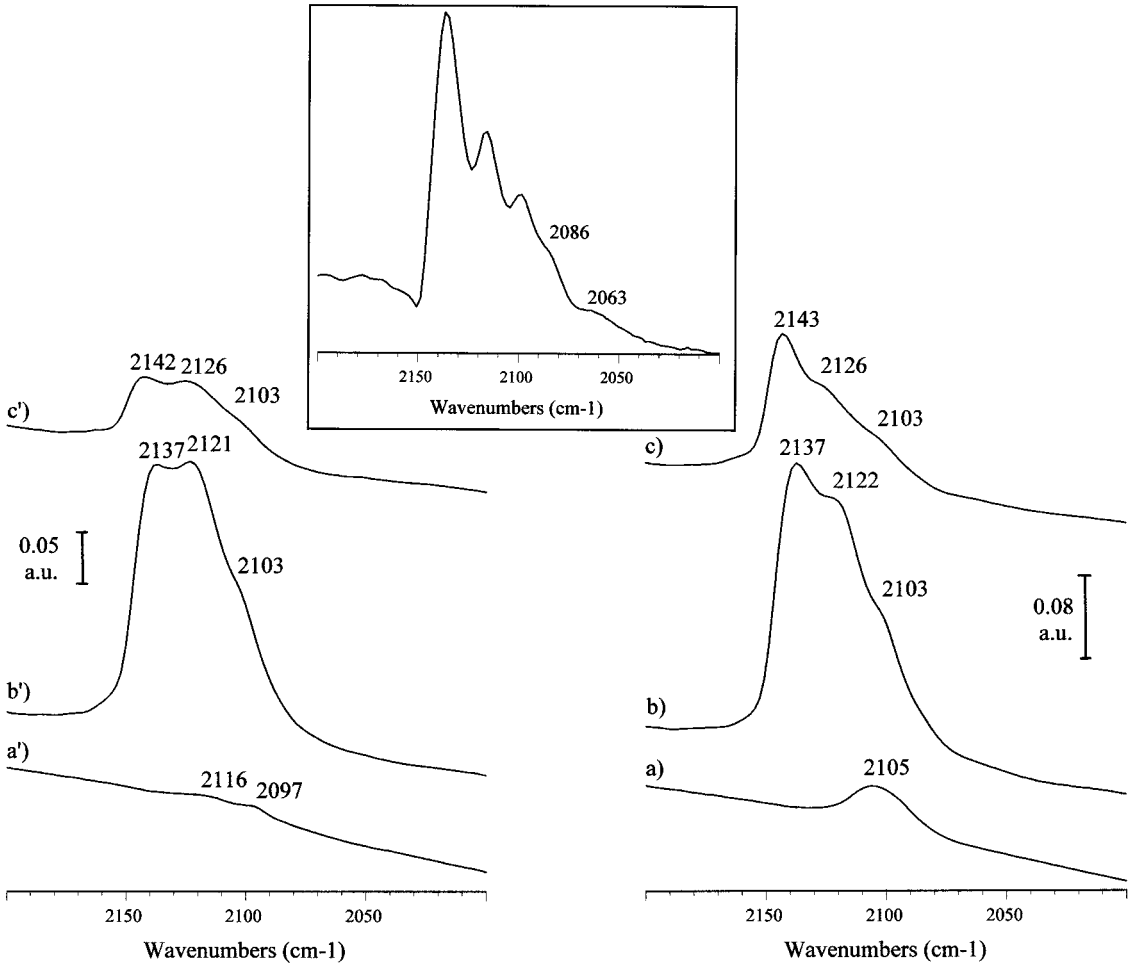

Figure 4. FTIR spectra following CO adsorption (10 Torr) at room temperature on CuCA (a−c) and CuA (a′−c′). (a, a′) initial calcined samples. Samples reduced at (b, b′) $T_r = 473$ K and (c, c′) $T_r = 573$ K. The inset shows the spectrum obtained by subtraction of b′ from b.

of the smaller bands at 2086 and 2063 cm^{-1} shown by CuCA can be attributed to species of the same type in which the copper particles are affected by interactions with the more basic ceria part of the support, as it has been proposed to explain similar shifts for Cu/MgO or Pd/CeO_2 catalysts.[26] Some doubts may exist with respect to the nature of the adsorption center for the

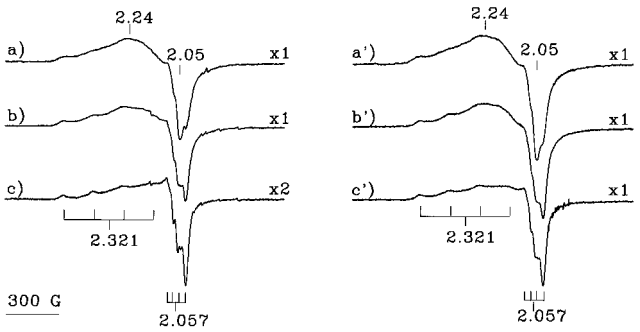

Figure 5. EPR spectra of CuCA (a−c) and CuA (a′−c′) (at 77 K). (a, a′) Initial calcined samples. Samples reduced in CO at (b, b′) 473 K and (c, c′) 573 K.

band observed in the initial calcined CuCA sample at 2105 cm^{-1}. Although it is in the wavenumber range of Cu^0 carbonyls, an alternative assignment might be made on the basis of the existence of interactions with the support,[26] and thus the possibility that it is due to Cu^+ carbonyls should be considered. On the other hand, bands appearing in the 2116−2143 cm^{-1} region are attributed to Cu^+−CO surface complexes.[18,25,26] The presence of several bands in this region indicates the existence of different types of Cu^+−CO complexes, differing in the state of the Cu^+ adsorption sites or, more precisely, in the environment of these sites. In this sense, an increase in the wavenumber of these species was proposed to indicate a higher concentration of Cu^{2+} ions in positions surrounding the Cu^+ adsorption site.[18,25] On this basis, bands appearing at 2135−2143 cm^{-1} in the CuCA or CuA samples are related to carbonyls adsorbed on Cu^+ sites located into a more oxidized environment than those giving bands at 2116−2126 cm^{-1}.

EPR Spectra. *(a) Detection and Evolution of Cu^{2+} Species.* Following calcination pretreatment and prolonged outgassing at room temperature of CuCA, the spectrum shown in Figure 5a was obtained. It is formed mainly by two overlapping Cu^{2+} signals: a broad anisotropic signal showing extremes at $g = 2.24$ and $g = 2.05$, signal A, and an axial, narrower one at $g_{\|} = 2.321$ and $g_{\perp} = 2.057$, signal B, in which a hyperfine pattern of four lines can be resolved in its two components, yielding coupling parameters $A_{\|} = 17.1 \times 10^{-3}$ cm^{-1} and $A_{\perp} = 1.9 \times 10^{-3}$ cm^{-1}. The relative contribution of signal A represents roughly 80% of the total spectrum intensity, as ascertained by simulating the full spectrum with a combination of both signals and evaluating their integrated intensities. Double integration of this experimental spectrum and comparison with a copper sulfate standard shows that about 55% of the total copper content is detected in it. When the spectrum is taken with sample under oxygen (equilibrium pressure at room temperature = 300 Torr), a large decrease of the overall intensity (so that only 30% remains) is produced, affecting mainly signal B; this indicates that most of the detected Cu^{2+} ions are located at the surface of the sample, those originating from signal B being more exposed. Minor signals, viz. a sextet of sharp lines centered at $g = 2.005$ and ascribable to Mn^{2+} impurities and an axial signal with $g_{\perp} = 1.967$ and $g_{\|} = 1.940$, due to electrons trapped on vacancies close to cerium cations or Ce^{3+} ions[27] and stabilized by the presence of cationic impurities,[12] are also observed in the spectra. Axial Cu^{2+} signals similar to those found in Cu/CeO_2 systems[28] were never discerned in the CuCA sample.

For sample CuA, spectra similar to those observed for CuCA are found in its initial calcined state (Figure 5a′); they show again the presence of mutually overlapping signals A and B. It is worth noting that for CuA a somewhat higher fraction of copper is detected in this initial EPR spectrum (63%). Careful inspection of the EPR spectra reveals some small differences between the spectra of CuCA and CuA in their initial states, mainly in the form of shoulders on the low-field parallel features, suggesting the presence of other smaller Cu^{2+} signals in CuCA samples, whose parameters (not very different from those found for sample CuA) cannot be determined with certainty and which might be related to Cu^{2+} species interacting to some extent with the ceria component of the CuCA sample.

CO adsorption at room temperature on CuA or CuCA resulted in a small overall intensity increase, larger for CuA than for CuCA. For higher T_r, up to $T_r = 573$ K, a progressive intensity decrease, which affects mainly signal A, is observed for both samples (Figure 5). After these thermal treatments in CO some more relevant differences are observed, since for CuA signal A decreases to a lower extent than for CuCA, which results in detection of a higher amount of Cu^{2+} after $T_r = 573$ K (28% of total copper for CuA vs 11% for CuCA).

Signal A, showing a relatively broad line width and, as a consequence, unresolved hyperfine splitting, must be due to Cu^{2+} species interacting with each other (i.e., broadly describable as clustered Cu^{2+} ions), where the signal is broadened by magnetic dipolar interactions (and, possibly, some spin exchange) between neighboring paramagnetic ions. On the other hand, signal B, in which hyperfine structure is well-resolved, can be attributed to isolated Cu^{2+} ions. Its EPR parameters are consistent with a tetragonally distorted octahedral symmetry; earlier studies on Cu/Al_2O_3 proposed a model for a similar signal in which Cu^{2+} was coordinated to five oxygen anions located at octahedral positions within a square-pyramidal configuration,[29] consistent with the proposed symmetry for these centers.

(b) Formation of Paramagnetic Oxygen Species. Oxygen adsorption (at a dose of ca. 70 μmol g^{-1}) at 77 K or room temperature on CuCA previously reduced in CO at $T_r = 373$ K produces a broadening of the spectrum; this affects mainly the resolution and intensity of signal B. No oxygen-derived signal (i.e., showing well-differentiated sharp features at g values close to $g_e \approx 2.0$) could be resolved, however, even by performing spectra subtraction in an attempt to cancel contributions of the dominant Cu^{2+} signals. Almost complete recovery of the initial spectrum is produced upon short outgassing at room temperature; this, along with the absence of oxygen radicals, shows clearly that the only relevant effect of oxygen adsorption at 77 K on the sample reduced at $T_r = 373$ K is the broadening beyond detection of the signals due to some Cu^{2+} cations by magnetic dipolar interactions with physisorbed molecular oxygen. A similar oxygen adsorption at 77 K or room temperature on the CuCA sample reduced at $T_r = 473$ K produces also a certain overall intensity decrease. However, in this case spectra subtraction clearly shows the appearance of a new signal with more or less symmetric line shape and located at $g = 2.020$ (Figure 6a). A better resolution of this signal is attained after oxygen adsorption at 77 K on CuCA treated at $T_r = 573$ K (Figure 6b). Computer simulation of this spectrum shows a major contribution of this signal with the following parameters: $g_z = 2.028$, $g_x = 2.017$, and $g_y = 2.011$, signal O1. This signal is similar to others detected upon O_2 adsorption on pre-outgassed Ce-containing systems.[12] To obtain a satisfactory computer simulation of this spectrum, in particular with respect to the amplitude and width proportions between the different spectrum features, it is, however, necessary to include, in addition to signal O1, a small contribution of an axial signal with $g_{\perp} = 2.026$ and $g_{\|} = 2.012$, signal O2. Parameters similar

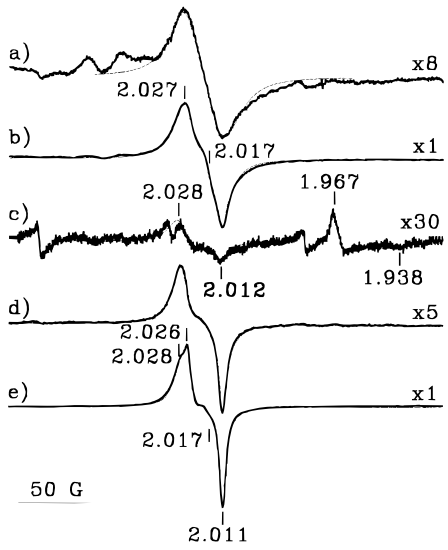

Figure 6. EPR spectra (at 77 K) following oxygen adsorption at 77 K on (a) CuCA reduced at $T_r = 473$ K, (b) CuCA reduced at $T_r = 573$ K, (c) CA reduced at $T_r = 373$ K, (d) CA reduced at $T_r = 473$ K, and (e) CA reduced at $T_r = 573$ K. For spectra a and b spectral subtraction was performed, attempting to cancel Cu^{2+} signals contributions. Computer-simulated spectra are overlapped as thinner lines.

to those of signal O1, though using somewhat broader components, allow to simulate satisfactorily the spectrum of Figure 6a.

To determine modifications of the characteristics of the oxygen signals induced by the presence of copper, the CA support has been examined in the same conditions as the CuCA sample (Figure 6c−e). Oxygen adsorption on the CA sample reduced at $T_r = 373$ K shows the presence of a small axial signal, similar to signal O2, though with slightly shifted parameters at $g_\perp = 2.027$ and $g_{||} = 2.012$ (Figure 6c). After oxygen adsorption on the sample reduced at $T_r = 473$ K, the spectrum shows an increase of signal O2, though the main contribution to the spectrum in these conditions still comes from signal O1 (now with the central feature at $g = 2.017$ significantly broadened) (Figure 6d). The presence of both signals O1 and O2 is apparent after oxygen adsorption on the sample reduced at $T_r = 573$ K (Figure 6e). In this case, addition of some contribution from a new signal O3, with $g_z = 2.032$, $g_x = 2.013$, and $g_y = 2.011$, is needed to obtain a satisfactory simulation of this spectrum. The relative magnitudes of the contributions of these signals to the spectra, obtained by computer simulation of the data in Figure 6, are summarized in Figure 7.

The parameters of signals O1, O2, and O3 are consistent with O_2^--Ce^{4+} species[12,30] formed by interaction of oxygen with reduced cerium centers. Signals O1 and O2, in particular, are characteristic of superoxide anions adsorbed on cerium centers closely interacting with the alumina support.[12] A plausible model on the structural characteristics of supported cerium oxide in these samples can be established on the basis of previous investigations correlating ceria dispersion with the characteristics of the observed EPR signals.[12] It was suggested there that a part of the ceria might be forming two-dimensional-like patches dispersed on the alumina surface, in which all cerium cations are interacting (via O bridges) with Al^{3+} cations, this being reflected in modifications of the EPR parameters of O_2^--Ce^{4+} radicals with respect to those observed on pure ceria.[30] Thus, signal O1 was proposed to be due to O_2^--Ce^{4+} species where the cerium adsorption centers are located at the surface of these patches, while signal O2 can be attributed to similar radicals

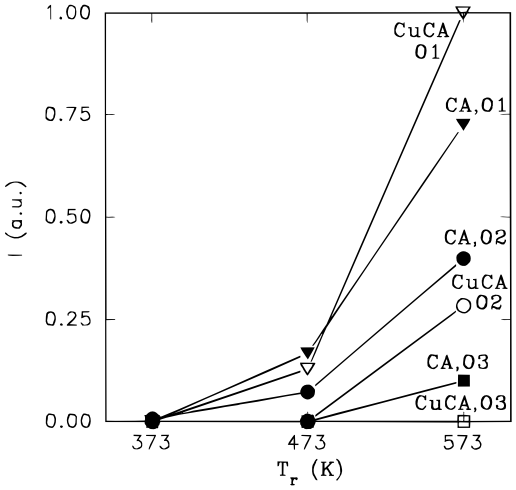

Figure 7. Contribution of signals O1, O2, and O3 extracted from the computer simulations of the EPR spectra of Figure 6, as a function of T_r.

where the cerium adsorption centers are at the edge of the patches. This assignment is in keeping with the assumption that the shift of g_x toward values higher than $g_x = 2.011$ (value typical for O_2^--Ce^{4+} on pure CeO_2) is related to the presence, in the first coordination sphere of the cerium adsorption center, of oxygen anions shared with aluminum cations rather than with other Ce ions; thus, the larger deviation of g_x for signal O2 suggests that the characteristics of this O_2^--Ce^{4+} species are dominated by the alumina surface to a higher extent than those of the superoxide species originating signal O1, as will be expected for positions at the edge of two-dimensional ceria patches. More detailed arguments on these assignments can be found elsewhere.[12] On the other hand, signal O3 is typical of superoxide species formed on large three-dimensional ceria particles;[30] observation of this signal correlates well with the observation of ceria peaks in the XRD of CA. The parameters and proposed assignments for the signals observed in this part of the study are collected in Table 2.

Discussion

Characteristics of the Catalysts in the Initial Calcined State. An important fraction of the whole copper content has been detected by EPR in the initial calcined CuA sample, revealing in turn that copper is present in at least two configurations with different dispersion degree: isolated Cu^{2+} ions (signal B) or clustered Cu^{2+} (signal A), the latter representing the largest fraction of the observed Cu. Due to the large line width of signal A (and the consequent absence of spectral details in it), it is difficult to evaluate the nature of the clustered Cu^{2+} entities on the basis of the analysis of the EPR signal alone. Previous studies on similar samples[31,32] suggest that these ions could be situated into local environments similar to those existing in pure copper oxide or in the copper aluminate spinel. However, it should in no case be considered that this signal corresponds to such pure phases in a bulk state, which would result in EPR-silent species (or lead to the detection of only a very small amount of defective Cu^{2+} ions)[33,34] due to strong magnetic interactions between Cu^{2+} ions. The formation of compounds closer to these pure phases might be the reason a part of copper is not detected by EPR in this calcined sample. In view of the important intensity decrease observed when the sample is placed under an oxygen atmosphere, signal A should be ascribed to Cu^{2+}-containing patches relatively dispersed on the alumina surface. Separate XPS experiments[35] on the initial

TABLE 2: Characteristics of the EPR Signals Observed in This Work[a]

signal	EPR parameters	proposed assignment
A	extremes at $g = 2.24$ and $g = 2.05$	Cu^{2+} located into a Cu^{2+}-containing surface dispersed phase (so-called clustered Cu^{2+})
B	$g_{\|\|} = 2.321$, $g_{\perp} = 2.057$, $A_{\|\|} = 17.1 \times 10^{-3}$ cm^{-1}, $A_{\perp} = 1.9 \times 10^{-3}$ cm^{-1}	isolated Cu^{2+} ions dispersed on alumina with square-pyramidal symmetry
O1	$g_z = 2.028-2.027$, $g_x = 2.017$, $g_y = 2.011$	$O_2^- - Ce^{4+}$ located at the surface of two-dimensional ceria patches dispersed on the alumina surface
O2	$g_{\perp} = 2.027-2.026$, $g_{\|\|} = 2.012$	$O_2^- - Ce^{4+}$ located at the edge of two-dimensional ceria patches dispersed on the alumina surface
O3	$g_z = 2.032$, $g_x = 2.013$, $g_y = 2.011$	$O_2^- - Ce^{4+}$ located at the surface of relatively large three-dimensional ceria particles

[a] Labeling of the g values for signals O1, O2, and O3 is chosen according to conventions of previous works,[12,30] which assign the z axis to the highest g value and the x axis to the component displaying the highest hyperfine splitting when ^{17}O-labeled oxygen is used.

CuA or CuCA samples have shown the presence of peaks due to Cu^{2+} at 935.4−935.7 eV, along with satellite peaks at ca. 944 eV, which point toward local environments for these ions similar to those in the copper aluminate spinel.[32] The increase of EPR intensity observed after adsorption of CO at room temperature indicates the presence in these samples of a third, less dispersed Cu^{2+}-containing phase not detected in the initial EPR spectra. This low-temperature adsorption could produce a small reduction of copper at the surface of these aggregates,[18] which would lead in turn to some decrease in the strong dipolar magnetic interactions between Cu^{2+} ions, thus allowing observation of part of the previously EPR-undetected Cu^{2+} species and giving rise to a moderate EPR intensity increase. In this sense, the FTIR results on CO adsorbed at room temperature on the initial calcined samples, showing the formation of a small amount of reduced copper carbonyls, might be related with these EPR observations.

In the case of CuCA, XRD results (summarized in Table 1) reveal the presence of peaks due to the fluorite structure of CeO_2 in the ceria-containing samples, thus evidencing the presence in this sample of relatively large ceria particles of the three-dimensional type (3D-Ce). On the other hand, EPR results after oxygen adsorption have shown in addition the formation of superoxide species characteristic of more dispersed ceria entities (so-called two-dimensional patches or 2D-Ce), thus evidencing the presence in this material of these entities, too. Therefore, the number of possible environments for the copper ions is higher in this sample than in CuA, since in addition to copper entities interacting with alumina, similar to those present in sample CuA, at least another two different copper entities interacting with 2D-Ce or 3D-Ce can be hypothesized to exist on CuCA.

The EPR spectrum of the initial calcined CuCA sample resembles much that shown by CuA, thus indicating that most of the detected Cu^{2+} cations interact with alumina. However, a lower overall amount of Cu^{2+} species is detected for calcined CuCA, suggesting that interactions with ceria stabilize a small part of the copper as EPR-silent species. In principle, such effects may be ascribed to the formation of particular diamagnetic Cu^{2+} aggregates in this sample or to the stabilization of some of the copper ions in an oxidation state lower than +2. FTIR spectra following CO adsorption on the calcined samples evidence a higher intensity of reduced copper carbonyls in calcined CuCA; as pointed out above, the carbonyl band responsible of this effect (appearing at 2105 cm^{-1}, Figure 4a) might be ascribed, taking into account the basic character of ceria, to Cu^+ carbonyls. There is still doubt, however, on whether this latter result should be attributed to the presence, already in the initial CuCA calcined sample, of reduced states of copper or to the presence of a particular Cu^{2+}-containing phase which would be easily reduced by interaction with CO at room temperature. The fact that this latter interaction leads to smaller changes in the amount of EPR-detected Cu^{2+} for the CuCA sample than for CuA suggests that the second interpretation is less likely. This is supported by previous reports,[9] based on XPS evidence, which propose that ceria stabilizes copper in a Cu^+ state already in preoxidized samples. On the other hand, it has also been observed that these effects are more pronounced as the amount of 3D-Ce particles is increased, unsupported ceria yielding the lowest Cu^{2+}/(total Cu) ratio in the EPR spectrum of the calcined sample and the highest FTIR intensity of a carbonyl band at ca. 2100 cm^{-1}.[10] Considering these previous results, it can be proposed that these variations in the behavior of sample CuCA, in comparison with sample CuA, are mainly due to the presence of copper ions interacting with relatively large ceria particles (3D-Ce), experiencing comparatively smaller interactions with the alumina carrier.

Further support for the existence of copper entities interacting with 3D-Ce is given by the absence of signal O3 in the EPR spectra of oxygen adsorbed on CuCA (Figure 7). This has been observed in some Cu/CeO_2 systems.[36] It could be due either to blocking of the corresponding cerium centers by copper entities or to the achievement of a deep ceria reduction produced by CO interaction with Cu−3D-Ce entities, which makes necessary to attain a certain degree of ceria reoxidation before O_2^--Ce^{4+} entities are stabilized.

On the other hand, the EPR results of Figures 6 and 7 show also that a part of the copper interacts with 2D-Ce entities. The intensity of O_2^--Ce^{4+} species obtained after oxygen adsorption on CuCA treated at $T_r \leq 473$ K, lower than that observed in the copper-free support treated in similar conditions, indicates a direct influence of copper on 2D-Ce, which hinders superoxide formation. The fact that oxygen adsorption produces no superoxide radical for CuCA at the lower T_r (373 K) while signals O1 and O2 begin to be formed at respectively $T_r = 473$ K and $T_r = 573$ K, suggests the existence of blocking phenomena in the calcined sample that disappear when the copper cations are reduced and migrate to form metal particles.

Behavior of the Catalysts upon Thermal Treatment in CO. CO-TPR of CuA shows low CO consumption levels for temperatures below ca. 573 K, indicating that a low extent of copper reduction is achieved in this temperature range. FTIR spectra of adsorbed CO indeed show that some copper reduction is produced in this T_r range, leading to the formation of Cu^+ or Cu^0 carbonyls upon CO adsorption. Probably, this moderate reduction affects mainly clustered Cu^{2+} species, taking into account that the EPR data obtained for this sample after similar treatments show that the intensity decrease affects mainly to the signal A component. This observation, along with the fact that larger Cu^{2+} aggregates likely begin to be reduced already at room temperature (as deduced from the increase in EPR signal, indicating decoupling of $Cu^{2+}-Cu^{2+}$), indicates that, as usually occurs in similar systems, the reducibility of alumina-supported Cu^{2+} decreases with increasing dispersion degree,

isolated Cu^{2+} ions being the least reducible. For $T \geq 573$ K, a higher CO consumption is observed in the CO-TPR experiment. The FTIR spectrum of adsorbed CO shows in turn an important decrease of the copper carbonyl bands for $T_r = 573$ K, which may be due to formation of large metallic copper particles,[18,37] in agreement with the mentioned higher degree of copper reduction detected in CO-TPR and with the larger decrease in EPR signal intensity. In summary, two different T_r ranges can be differentiated in the behavior toward CO reduction of Cu^{2+} in CuA. In the first one, up to ca. 573 K, a slow copper reduction process leads to generation of some Cu^+ and Cu^0 entities; in a second one, for $T_r \geq$ ca. 573 K, a deeper reduction level of copper is achieved, leading mainly to formation of large metallic copper particles.

For sample CuCA, a shift to lower temperature is observed in the first important CO consumption step in the CO-TPR experiment (Figure 1). Since cerium can be involved in these processes as well, deriving data on Cu reduction from these results is less straightforward, so it is necessary to consider the outcome of the other techniques used. The main features of the FTIR spectrum of adsorbed CO (Figure 4) are related to copper entities interacting with alumina rather than with ceria-related entities, in agreement with EPR results. However, from the comparison of the intensity of the FTIR spectra of adsorbed CO of Figures 4b,b′ (observed more clearly in the inset of Figure 4), as well as from the EPR results of Figure 5, that the reduction level that can be attained in the range $T_r < 573$ K in this CuCA sample is higher than in CuA. This suggests that there is a certain assistance by reduced ceria entities to the copper reduction process (maybe via electron transfers or related phenomena). Actually, the difference spectrum in Figure 4 (inset) does show that additional Cu^0 particles are formed on CuCA for $T \leq 473$ K that yield new carbonyls upon CO adsorption (bands at 2086 and 2063 cm^{-1}) which do not form in CuA. These wavenumbers, lower than those of Cu^0 carbonyls observed on more acid supports,[24] indicate that the corresponding $CO-Cu^0$ entities undergo significant interactions with a basic support;[26] this suggests that the corresponding copper entities interact with ceria. Taking into account that the basicity of ceria is nearly eliminated by its dispersion on alumina,[13] it seems likely that these lower FTIR wavenumbers arise from copper interacting with 3D-Ce rather than with 2D-Ce.

These considerations can be coupled with the EPR results on the formation of superoxide species, which originate following the process (using formal charges) $Ce^{3+} + O_2 \rightarrow Ce^{4+}$-$O_2^-$. For CuCA, these data show that reduction of 2D-Ce is produced for $T_r \geq 473$ K; this result correlates well with the observation of a first step of CO consumption in the CO-TPR of CuCA (Figure 1) starting at ca. 423 K, which is comparatively larger than the CO consumption steps observed for CuA for T_r below 773 K, and thus suggests that significant ceria reduction is involved. Considering that, as evidenced by similar studies on a Cu/CeO_2 catalyst,[36] 3D-Ce entities are strongly reduced by CO even at $T_r \leq 373$ K, the observation of similar effects in the alumina-supported material at a relatively higher T_r (≥ 423 K) is likely to be related to phenomena involving dispersed 2D-Ce entities. In this sense, the higher amount of reduced copper carbonyls detected for CuCA at $T_r = 473$ K might be connected to the formation of mixed oxide phases of the type $(Cu,Ce)AlO_{3-x}$, recently proposed to exist in similar materials,[38] which would stabilize copper in a Cu^+ oxidation state.

As an additional comment it can be said that CO disproportionation, leading to carbon deposition, might be produced during the TPR runs, contributing in an important way to the steps seen to occur starting at ca. 773 K in the TPR profiles of both CuA and CuCA samples. This hypothesis can be based on the results of the TPO-TPD experiments shown in Figure 2. Since oxidation of reduced supported copper is expected to occur at T < 700 K,[39] the observation of a large CO_2 production for $T >$ ca. 773 K can be attributed to oxidation of a strongly adsorbed species, like deposited carbon.[40] According to the previous arguments, active centers for the Boudouard reaction are probably metallic copper particles,[41] produced during the last part of the TPR runs.

Conclusions

EPR data on a preoxidized Cu/Al_2O_3 catalyst evidence the presence of two distinct oxidized copper entities, i.e., clustered Cu^{2+} and isolated Cu^{2+} ions; a third Cu^{2+}-containing aggregate phase, yielding EPR-silent species, is assumed to exist on the basis of the increase of EPR intensity upon CO adsorption at room temperature. The behavior of these entities in respect to reduction by CO shows that their reducibility decreases with the degree of dispersion on the alumina surface. Two different ranges of reduction in CO are detected for Cu/Al_2O_3 with a turning point at $T_r =$ ca. 573 K. For a lower T_r, the CO-TPR profile shows that a small reduction level is achieved leading to the formation of different Cu^+ and Cu^0 species, evidenced by the formation of particular carbonyls in the FTIR spectra of adsorbed CO; for higher T_r, CO-TPR reveals a more strong reduction process, leading probably to formation of large metallic copper particles, in view of the apparent decrease of copper carbonyls evidenced by FTIR of adsorbed CO.

Important similarities, in comparison with the Cu/Al_2O_3 sample, are observed in the behavior toward CO reduction of copper in the $Cu/CeO_2/Al_2O_3$ sample, showing that a large fraction of copper in this sample interacts with alumina, as revealed also by comparison of the EPR spectra of the initial samples. The $Cu/CeO_2/Al_2O_3$ sample shows, however, new copper entities that interact with ceria entities; this is evidenced by a lower intensity of Cu^{2+} EPR signals in the initial calcined sample, with respect to Cu/Al_2O_3, and by the formation of a carbonyl species giving a FTIR band at 2105 cm^{-1} upon CO interaction at room temperature. This indicates the stabilization, in the presence of ceria, of diamagnetic states of copper, which involve either reduced states (probably Cu^+) or a Cu^{2+}-containing phase easily reduced by interaction with CO at room temperature. These copper entities are most easily reduced by CO, yielding metallic particles for $T_r \leq 473$ K, as revealed by formation of carbonyls at 2086 and 2063 cm^{-1} in the FTIR spectrum of adsorbed CO, and are attributed to copper species that interact with large three-dimensional ceria particles. This easier reduction of copper on these particles can contribute in an important way to the high activity for CO oxidation shown by Cu/CeO_2.[10] On the other hand, contacts of copper with dispersed two-dimensional ceria are evidenced by EPR of adsorbed oxygen. These two-dimensional ceria entities are proposed to assist in the copper reduction process, as revealed by the lower intensity of clustered Cu^{2+} in the EPR spectra at $T_r \geq 473$ K and the higher intensity of carbonyl bands in the FTIR spectrum of adsorbed CO at $T_r = 473$ K.

Acknowledgment. Financial support of this work under CICYT project MAT94-0835-C03-02 is gratefully acknowledged. Mr. F. Sánchez Constenla is also acknowledged for recording some of the EPR spectra. Thanks are due to Mrs. L. Bajón and Prof. J. M. Palacios for performing the SEM-EDAX experiments and to Mrs. M. Garrido for the XRD experiments.

References and Notes

(1) (a) Harrison, B.; Diwell, A. F.; Hallett, C. *Platinum Met. Rev.* **1988**, *32*, 73. (b) Leclercq, G.; Dathy, C.; Mabilon, C.; Leclercq, L. *Stud. Surf. Sci. Catal.* **1991**, *71*, 181. (c) Heck, R. M.; Farrauto, R. J. In *Catalytic Air Pollution Control; Commercial Technology*; Van Nostrand Reinhold: New York, 1995.

(2) (a) Dictor, R.; Roberts, S. *J. Phys. Chem.* **1989**, *93*, 5846. (b) Su, E. C.; Rothschild, W. G. *J. Catal.* **1986**, *99*, 506.

(3) (a) Yao, H. C.; Yu Yao, Y. F. *J. Catal.* **1984**, *86*, 254. (b) Engler, B.; Koberstein, E.; Schubert, P. *Appl. Catal.* **1989**, *48*, 71. (c) Miki, T.; Ogawa, T.; Haneda, M.; Kakuta, N.; Ueno, A.; Tateishi, S.; Matsuura, S.; Sato, M. *J. Phys. Chem.* **1990**, *94*, 6464.

(4) (a) Shido, T.; Iwasawa, Y. *J. Catal.* **1992**, *136*, 493. (b) Shido, T.; Iwasawa, Y. *J. Catal.* **1993**, *141*, 71.

(5) Martínez-Arias, A.; Soria, J.; Conesa, J. C.; Seoane, X. L.; Arcoya, A.; Cataluña, R. *J. Chem. Soc., Faraday Trans.* **1995**, *91*, 1679.

(6) (a) Hardacre, C.; Ormerod, R. M.; Lambert, R. M. *J. Phys. Chem.* **1994**, *98*, 10901. (b) Putna, E. S.; Vohs, J. M.; Gorte, R. J. *J. Phys. Chem.* **1996**, *100*, 17862.

(7) Trovarelli, A. *Catal. Rev.—Sci. Eng.* **1996**, *38*, 439 and references therein.

(8) Shaw, E. A.; Rayment, T.; Walker A. P.; Lambert, R. M. *Appl. Catal.* **1990**, *67*, 151.

(9) (a) Liu, W.; Sarofim, A. F.; Flytzani-Stephanopoulos, M. *Chem. Eng. Sci.* **1995**, *49*, 4871. (b) Liu, W.; Flytzani-Stephanopoulos, M. *J. Catal.* **1995**, *153*, 304.

(10) Martínez-Arias, A.; Soria, J.; Cataluña, R.; Conesa, J. C.; Cortés Corberán, V. *Preprints of the 4th International Congress on Catalysis and Automotive Pollution Control (CAPoC4) Congress* (*Brussels, 1997*); Vol. 2, p 271.

(11) Shyu, J. Z.; Weber, W. H.; Gandhi, H. S. *J. Phys. Chem.* **1988**, *92*, 2561.

(12) Soria, J.; Coronado, J. M.; Conesa, J. C. *J. Chem. Soc., Faraday Trans.* **1996**, *92*, 1619.

(13) Morterra, C.; Bolis, V.; Magnacca, G. *J. Chem. Soc., Faraday Trans.* **1996**, *92*, 1991.

(14) Cordatos, H.; Ford, D.; Gorte, R. J. *J. Phys. Chem.* **1996**, *100*, 18128.

(15) Jernigan, G. G.; Somorjai. G. A. *J. Catal.* **1994**, *147*, 567.

(16) Cataluña, R. Ph.D. Thesis, Universidad Politécnica de Madrid, 1995.

(17) Hierl, R.; Knözinger, H.; Urbach, H.-P. *J. Catal.* **1981**, *69*, 475.

(18) Padley, M. B.; Rochester, C. H.; Hutchings, G. J.; King, F. *J. Catal.* **1994**, *148*, 438.

(19) Knözinger, H.; Ratnasamy, P. *Catal. Rev.—Sci. Eng.* **1978**, *17*, 31.

(20) Ballinger, T. H.; Yates Jr., J. T. *Langmuir* **1991**, *7*, 3041.

(21) Morterra, C.; Bolis, V.; Magnacca, G. *Langmuir* **1994**, *10*, 1812.

(22) Busca, G. *J. Mol. Catal.* **1987**, *43*, 225.

(23) (a) Solymosi, F.; Erdöhelyi, A.; Kocsis, M. *J. Catal.* **1980**, *65*, 428. (b) Solymosi, F.; Pásztor, M. *J. Catal.* **1987**, *104*, 312.

(24) Hollins, P. *Surf. Sci. Rep.* **1992**, *16*, 51 and references therein.

(25) Lokhov, Y. A.; Sadykov, V. A.; Tikhov S. F.; Popovskii. V. V. *Kinet. Katal.* **1985**, *26*, 177.

(26) (a) Davydov, A. A. *Kinet. Katal.* **1985**, *26*, 157. (b) Bensalem, A.; Muller, J.-C.; Tessier, D.; Bozon-Verduraz, F. *J. Chem. Soc., Faraday Trans.* **1996**, *92*, 3233.

(27) Che, M.; Tench, A. J. *Adv. Catal.* **1983**, *32*, 1.

(28) Soria, J.; Conesa, J. C.; Martínez-Arias, A.; Coronado, J. M. *Solid State Ionics* **1993**, *63−65*, 755.

(29) Berger P. A.; Roth, J. F. *J. Phys. Chem.* **1967**, *71*, 4307.

(30) Soria, J.; Martínez-Arias, A.; Conesa, J. C. *J. Chem. Soc., Faraday Trans.* **1995**, *91*, 1669.

(31) Friedman, R. M.; Freeman, J. J.; Lytle, F. W. *J. Catal.* **1978**, *55*, 10.

(32) Tikhov, S. F.; Sadykov, V. A.; Kryukova, G. N.; Paukshtis, E. A.; Popovskii, V. V.; Starostina, T. G.; Kharlamov, G. V.; Anufrienko, V. F.; Poluboyarov, V. F.; Razdobarov, V. A.; Bulgavov N. N.; Kalinkin. A. V. *J. Catal.* **1992**, *134*, 506.

(33) Singh, R. J.; Punnoose, A.; Mathew, J.; Maruya, B. P.; Umar, M.; Haque, M. I. *Phys. Rev. B* **1994**, *49*, 1346.

(34) Yu, J.-T.; Hwang, J. G.; Tsai, C.-C.; Lii, K. H. *Solid State Commun.* **1989**, *70*, 167.

(35) Martínez-Arias, A., unpublished results.

(36) Martínez-Arias, A.; Soria, J.; Conesa, J. C. Manuscript in preparation.

(37) Sepúlveda, A.; Márquez, C.; Rodríguez-Ramos, I.; Guerrero-Ruíz, A.; Fierro, J. L. G. *Surf. Interface Anal.* **1993**, *20*, 1067.

(38) Fernández-García, M.; Gómez-Rebollo, E.; Guerrero Ruiz, A.; Conesa, J. C.; Soria, J. *J. Catal.* **1997**, *172*, 146.

(39) Kohler, M. A.; Curry-Hyde, H. E.; Hughes, A. E.; Sexton, B. A.; Cant, N. W. *J. Catal.* **1987**, *108*, 323.

(40) Querini, C. A.; Fung, S. C. *Appl. Catal. A* **1994**, *117*, 53.

(41) Jagannathan, K.; Srinivasan, A.; Hedge, M. S.; Rao, C. N. R. *Surf. Sci.* **1980**, *99*, 309.